International Journal of Bifurcation and Chaos, Vol. 17, No. 9 (2007) 3071–3083

COMPLEX BIFURCATION STRUCTURES IN THE HINDMARSH–ROSE NEURON MODEL

J. M. GONZÁLEZ-MIRANDA
Departamento de Física Fundamental, Universidad de Barcelona, Avenida Diagonal 647, Barcelona 08028, Spain

Received June 12, 2006; Revised October 25, 2006

The results of a study of the bifurcation diagram of the Hindmarsh–Rose neuron model in a two-dimensional parameter space are reported. This diagram shows the existence and extent of complex bifurcation structures that might be useful to understand the mechanisms used by the neurons to encode information and give rapid responses to stimulus. Moreover, the information contained in this phase diagram provides a background to develop our understanding of the dynamics of interacting neurons.

Keywords: Neuronal dynamics; neuronal coding; deterministic chaos; bifurcation diagram.

1. Introduction

There are two main problems in neuroscience whose solution is linked to the research in nonlinear dynamics and chaos. One is the problem of integrated behavior of the nervous system [Varela *et al.*, 2001], which deals with the understanding of the mechanisms that allow the different parts and units of the nervous system to work together, and appears related to the synchronization of nonlinear dynamical oscillators. The other is the neural coding problem [Sejnowski, 1995; Abeles, 2004], which is aimed to know how the neurons encode the information that they transmit and exchange in the working of the nervous system, and is related to both, the knowledge of the different types of dynamics available to nonlinear dynamical systems and to chaos synchronization.

The theoretical study of such problems, in its most basic aspects, partly relies on mathematical models of the electrophysics of a single neuron, most of them developed from the pioneering work by Hodgkin and Huxley [1952]. Among them, the model by Hindmarsh and Rose [1984], which is the result of a mapping of the Hodgkin–Huxley model to a relatively simple nonlinear oscillator [Fitzhugh, 1961] has proven to give a good qualitative description of the dynamics of the membrane potential of a single neuron, which is the most relevant experimental output of the neuron dynamics. Because of the enormous development that the field of dynamical systems and chaos has undergone in the last thirty years [Hirsch *et al.*, 2004; Ott, 2002], the study of meaningful mathematical systems like the Hindmarsh–Rose model have acquired new interest [Holmes, 2005] because of the new information that can now be obtained from them.

In particular, it has been found recently that the dynamics of this system, when studied as a function of significant control parameters, presents two relevant features: (i) continuous interior crisis [González-Miranda, 2003], which are abrupt changes in the nature of the dynamics of the system attractor, and (ii) block structured dynamics [González-Miranda, 2005], which is a complex bifurcation structure where the dynamics available to the system are grouped in blocks of alike periodicity. The first of these items provides a potential mechanism for rapid responses in the nervous system by switching between different dynamical behaviors. The second provides structures that appear as

possible basic elements to encode messages in the apparently random trains of action potentials that run along the axon of an activated neuron.

These two phenomena have received detailed study at particular restricted values of the Hindmarsh–Rose model parameters. The aim of the present paper is to report a comprehensive study of the manifestation of these phenomena for a wide range of system parameters; that is, to provide a phase diagram of the Hindmarsh–Rose model, which gives a global view of the availability of these and other dynamical behaviors to this system.

This article is arranged as follows. After this introduction, in Sec. 2, we give a basic description of the complexities in the bifurcation diagrams of the Hindmarsh–Rose neuron model. In Sec. 3, we present the results of a linear stability analysis in a wide and significant region of the parameter space. In Sec. 4, we analyze stability from the nonlinear point of view by means of the use of Lyapunov exponents, and go further in the nonlinear analysis giving a global view of the bifurcation diagrams. In Sec. 5, we provide evidence for the structural stability of the above results, and finally, in Sec. 6 we discuss and summarize the main conclusions of the paper.

2. Complex Bifurcation Structures

The Hindmarsh–Rose model describes the dynamics of the membrane potential in the axon of a neuron, $x(t)$, by means of a three-dimensional system of nonlinear first-order differential equations, which written in dimensionless form read:

$$\dot{x} = y + 3x^2 - x^3 - z + I, \tag{1}$$

$$\dot{y} = 1 - 5x^2 - y, \tag{2}$$

$$\dot{z} = r\left[4\left(x + \frac{8}{5}\right) - z\right]. \tag{3}$$

The other two dynamical variables, $y(t)$ and $z(t)$, describe the exchange of ions through the neuron membrane by means of fast and slow ion channels, respectively. The main parameters of the model are the current that enters the neuron, I, and the efficiency of the slow channels to exchange ions, r.

The dynamics that one can observe for the action potential, $x(t)$, are quite diverse as illustrated in Fig. 1. There are equilibrium solutions where the action potential decays to a constant value, as shown in Fig. 1(a), as well as a variety of

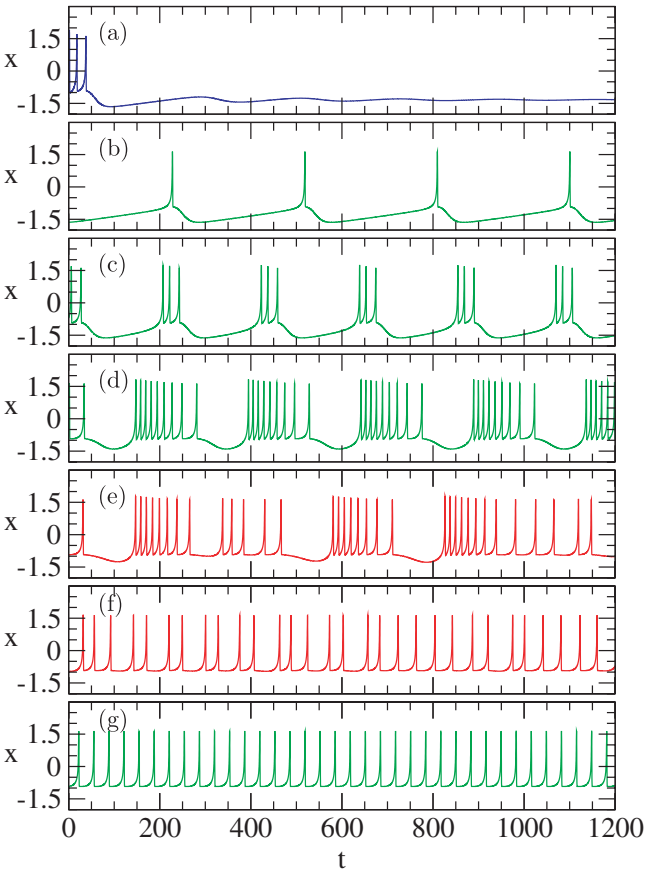

Fig. 1. Time series for the action potential for the Hindmarsh–Rose model for $r = 0.003$ and different values of the current applied: (a) $I = 1.26$, (b) $I = 1.28$, (c) $I = 1.67$, (d) $I = 3.20$, (e) $I = 3.29$, (f) $I = 3.34$, and (g) $I = 3.50$.

oscillatory solutions than can be simple periodic firings of a single spike [Figs. 1(b) and 1(g)], periodic firings of well-defined bursts of spikes [Figs. 1(c) and 1(d)], or chaotic firings of spikes and bursts of spikes [Figs. 1(f) and 1(e)]. Most of these dynamical behaviors being oscillatory, they can be characterized by means of the time intervals between consecutive peaks, T_i $(i = 1, 2, \ldots, N)$, for each function $x(t)$. In neurobiology, these time intervals, T_i, are known as inter-spike intervals, and it is believed that in the structure of inter-spike intervals is where neurons encode the information [Sejnowski, 1995; Abeles, 2004]. Therefore, they are the relevant observables for neuronal dynamics; because of this, they will be our basic observables here.

We have used them to construct one-dimensional bifurcation diagrams as those presented in Fig. 2. These have been obtained through the numerical integration of the equations of motion, Eqs. (1)–(3), by means of a fourth-order Runge–Kutta algorithm with time step 0.005. The

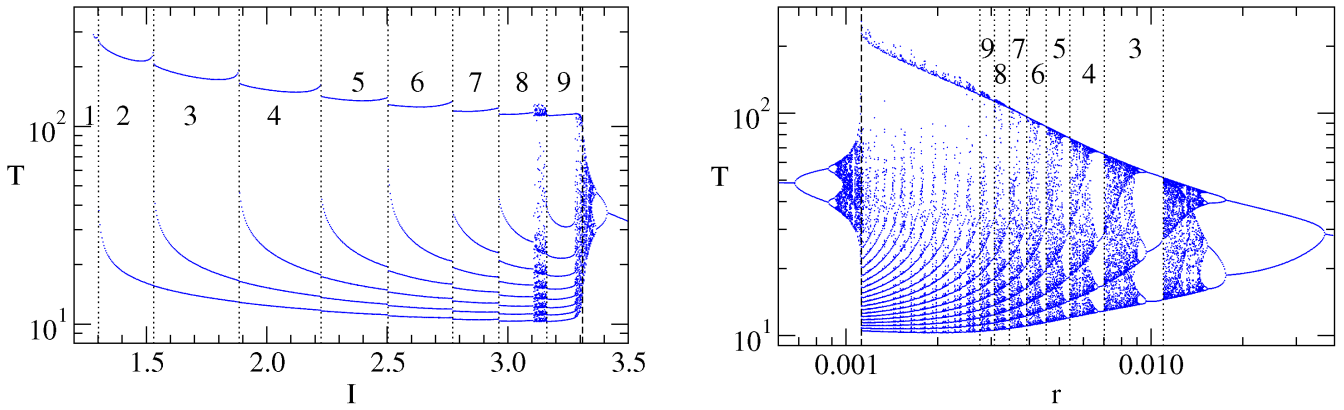

Fig. 2. Two examples of bifurcation diagrams computed for different bifurcation parameters: (a) for I changing and r fixed ($r = 0.003$), and (b) for r changing and I fixed ($I = 3.25$). A vertical dashed line signals the point where the continuous interior crisis occurs, and vertical dotted lines separate the blocks, identified by its periodicity number, p. For (b) only a selected set of blocks of low periodicity have been signaled to avoid having the figure cluttered up with dotted lines.

value of one of the system parameters, r or I, was fixed, and time series solutions were obtained for a set of different values of the other parameter, which is considered a bifurcation parameter. Then, plotting as dots the different values of T_i obtained for each of the values given to the bifurcation parameter, the bifurcation diagrams were obtained. We will note that the conclusions that follow would had been the same if more conventional observables to construct the bifurcation diagrams, such as the maxima of $x(t)$ or the times of crossing a surface in phase space, had been used.

Representative results of what is obtained for fixed r, and taking I as bifurcation parameter appear in Fig. 2(a). In this case, the value of r is taken as 0.003, which is the same used to obtain the time series shown in Fig. 1. This bifurcation diagram provides an illustration of two potentially biologically significant bifurcation structures: continuous crises [González-Miranda, 2003], and block structured dynamics [González-Miranda, 2005].

A continuous crises shows up as a sharp change in the width of the bifurcation diagram at $I_C \approx 3.31$. To the right of the crisis, we have the well-known bifurcation structure of an inverted period doubling cascade. A continuous interior crisis is a chaos–chaos transition between two qualitatively different dynamical behaviors in phase space. On the side where the bifurcation diagram is narrow we have spiking dynamics, characterized by an irregular firing of spikes like the one shown in Fig. 1(f). In the wide part there is bursting dynamics, which is a complex dynamical behavior where bursts of spikes are separated by lapses of quiescence [Fig. 1(e)]. The dynamics in the spiking regime is characterized by one time scale, that of the spikes, while in the bursting regime there are two time scales, one for the bursts and other for the spikes. The transition between these two dynamical regimes is what is called a continuous interior crisis. For a detailed qualitative and quantitative study of the these crisis the reader is referred to [González-Miranda, 2003].

Block structured dynamics is observed to the left of the bifurcation diagram, for $1.28 \leq I \leq 3.31$. In this case the dynamical behaviors available can be classified in blocks accordingly to its periodicity, p. Each block can be defined giving a segment of I where all motions have the same periodicity, and whose limits are period-adding bifurcations. For $I < 1.28$ the dynamics falls to a fixed point, being the interval for $p = 1$ very small $I \in [1.28, 1.30]$. It deserves to be noted that the dynamics within a block can be purely periodic, as observed here for the blocks of low periodicity, or may have chaotic regions inside, as displayed for the blocks of large periodicity. In these chaotic regions, the average values of the periodicity, as well as of other statistical measures of the distribution of the inter-spike intervals are similar to those of the periodic part of the block where they belong. A detailed study of block structures dynamics can be found in [González-Miranda, 2005]. Figures 1(a)–1(g) further illustrate all this: in Fig. 1(a) we see the decay to the equilibrium, in Figs. 1(b)–1(d) we have examples of periodic motions in blocks $p = 1, 3, 9$,

respectively. Figure 1(e) shows the chaotic dynamics in the region of periodicity $p = 9$, and Figs. 1(f) and 1(g) the chaotic and period-1 dynamics after the continuous crisis, respectively.

A bifurcation diagram when r is taken as the bifurcation parameter is shown in Fig. 2(b) which corresponds to $I = 3.25$. In this case, a continuous interior crisis, which is very sharp, occurs for small values of the bifurcation parameter. Period adding bifurcations develop as r decreases and a large number of different blocks are observed, while chaos occurs mainly within the blocks of low periodicity here. Although the same type of dynamic behaviors seen for fixed r also appear in this case, they occur in a somewhat different way.

3. Linear Stability Analysis

The results in the above section reveal a variety of dynamical behaviors in the Hindmarsh–Rose model: there are equilibria and oscillations, the oscillations can be of a variety of types depending on their periodicity, and there is chaos. It is then interesting to investigate how they are distributed along its two-dimensional space of parameters, $r - I$. Most of the research reported on this model has been done giving numerical values to $I \approx 3$, and to $r \approx 0.006$ or $r \approx 0.001$, as can be seen, for example, in the papers by Dhamala *et al.* [2004], Huang [2004] and Percha *et al.* [2005], to name a few of the most recent references on research where the Hindmarsh–Rose model plays a relevant role. This is a limited set of parameter values, mainly if one takes into account that Hindmarsh and Rose [1984] studied the dynamics for four values for these parameters (including the above) that were scattered within the ranges $-3.0 \leq I \leq 4.0$ and $0.001 \leq r \leq 0.005$.

In this paper, we report the results of a systematic study of the dynamical behaviors available to the Hindmarsh–Rose model in a rectangle

$$\mathcal{R} = \{(r, I) | r \in [10^{-4}, 0.05] \text{ and } I \in [-8.0, 8.0]\}, \tag{4}$$

whose edges are the segments $[10^{-4}, 0.05]$ and $[-8.0, 8.0]$, for r and I, respectively. This is a region of the parameter space that, regarding the two parameters, is larger than the region where Hindmarsh and Rose [1984] performed their study. We note, however, that the upper limit that we consider for r is still small enough so that Eq. (3) can be a description of the dynamics of slow ion channels, and the values for I are still within realistic ranges. To consider the change of these parameters is meaningful. To change I in a certain interval means to change the intensity of the current injected in the neuron. The variation of r allows two interpretations. On one side, different values of r might refer to consider different neurons, having each different densities of slow ion channels in their axon membranes. To allow a relatively wide range of variation for r is meaningful because neurons can be of many different types, and to present a great variability between individuals. A second reason for changing r is to take into account the existence of ionic channels that can be chemically activated or deactivated, so that the permeability of the axon membrane of a given neuron can be modified by means of the presence or absence of the appropriate activating–deactivating chemical. The variations of r would then take into account this possibility.

We start our study of the two-dimensional bifurcation diagram with a linear stability analysis of Eqs. (1)–(3). They have a single fixed point (i.e. equilibrium) which is determined by the only real root of the polynomial

$$p(x) = x^3 + 2x + 4x + \left(\frac{27}{5} - I\right), \tag{5}$$

which depends on I but not on r. The real root, $x_F(I)$, determines the other coordinates of the fixed point by means of

$$\begin{aligned} y_F(I) &= 1 - 5x_F^2(I), \\ z_F(I) &= 4x_F(I) + \frac{32}{5}. \end{aligned} \tag{6}$$

The stability of this equilibrium is given by the eigenvalues of the Jacobian matrix

$$J = \begin{pmatrix} 6x - 3x^2 & 1 & -1 \\ -10x & -1 & 0 \\ 4r & 0 & -r \end{pmatrix} \tag{7}$$

of the flow [Eqs. (1)–(3)], which are the roots of its characteristic polynomial:

$$P(\Lambda) = \Lambda^3 + a(r, I)\Lambda^2 + b(r, I)\Lambda + c(r, I), \tag{8}$$

being the coefficient functions of r and I:

$$a(r, I) = 1 + r - 6x_F(I) + 3x_F^2(I), \tag{9}$$

$$\begin{aligned} b(r, I) = {} & [5 - 6x_F(I) + 3x_F^2(I)]r \\ & + 4x_F(I) + 3x_F^2(I), \end{aligned} \tag{10}$$

$$c(r, I) = [4 + 4x_F(I) + 3x_F^2(I)]r. \tag{11}$$

We have determined $x_F(I) \in \mathbb{R}$ and $\Lambda(r, I) \in \mathbb{C}$ as the roots of $p(x) = 0$ and $P(\Lambda) = 0$, respectively. These have been computed exactly as the solutions of these cubic equations obtained by radicals, using the Cardano–Vieta formulas [Birkhoff & Mac Lane, 1996]. The results for $x_F(I)$, presented in Fig. 3 show a monotonous increase of $x_F(I)$ within a narrow range of values; while, $z_F(I)$, also increases, although in wider range, and $y_F(I)$ is the variable which suffers a larger variation, this increases for $I \lesssim 5.0$ and decreases slightly for $I \gtrsim 5.0$.

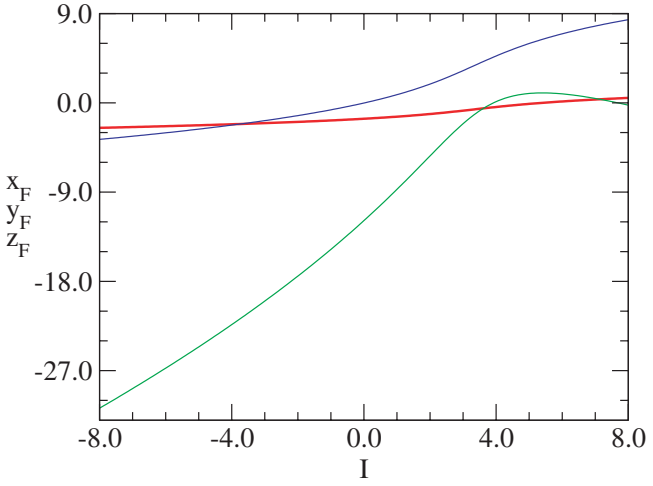

Fig. 3. The only real root, $x_F(I)$, of $x^3+2x+4x+[(27/5)-I] = 0$ (red line), and the other coordinates of the fixed point, $X_F = (x_F, y_F, z_F)$, of Eqs. (1)–(3), determined from it: $y_F(I)$ (green line), and (c) $z_F(I)$ (blue line).

Regarding $\Lambda(r, I)$, we have obtained a first eigenvalue $\Lambda_1(r, I)$ which is real and negative for all $(r, I) \in \mathcal{R}$, and two complex conjugate eigenvalues, $\Lambda_2(r, I)$ and $\Lambda_3(r, I)$, whose real and imaginary parts contain the essential information to classify the equilibrium. All eigenvalues found have no zero real parts, so we conclude that the system is hyperbolic in $\mathcal{R}$; therefore, the nonlinear dynamics near the equilibrium point resemble the linearized system [Hirsch *et al.*, 2004]. The results for the eigenvalues are summarized in Fig. 4 where the real and imaginary parts of $\Lambda_2(r, I)$ are displayed as 3D-color plots. The plot [Fig. 4(a)] of the real part of the second eigenvalue, $\mathbb{R}e[\Lambda_2(r, I)]$, which is identical to that of $\mathbb{R}e[\Lambda_3(r, I)]$ (not displayed), shows that $\mathcal{R}$ is separated in four regions which have approximately the shape of horizontal strips which we will name from bottom to top as regions A, B, C and D. In this figure, regions A and C appear colored violet-blue, and regions B and D orange-red.

For increasing values of I, they are as follows (see Fig. 5). For negative and small positive values of I, we have region A, which is characterized by $\mathbb{R}e[\Lambda_{2,3}(r, I)] < 0$. This region occurs for values of I below a certain curve $I = \phi_A(r)$ that increases monotonously within the interval $I \in [1.2, 2.0]$. This line is visualized as the edge between the lower blue and orange regions. In region B, it is $\mathbb{R}e[\Lambda_{2,3}(r, I)] > 0$ for a range of values of I that are above $\phi_A(r)$ and below and almost a horizontal line, $I = \phi_B(r)$, that occurs around $I \approx 5.2$ (again as the edge between orange and blue regions). Region C,

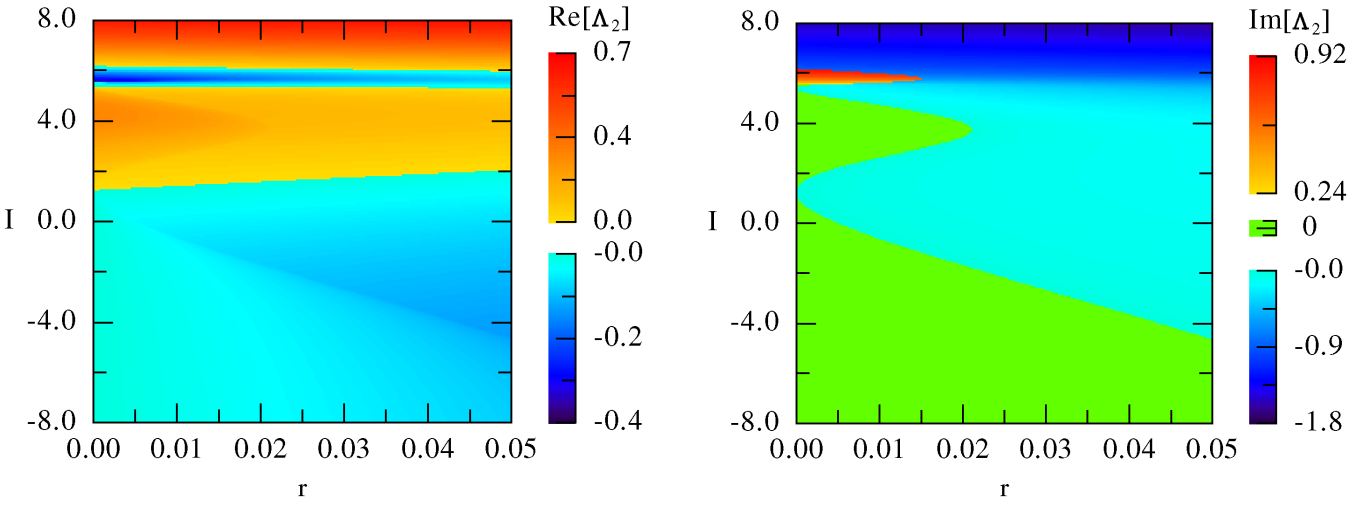

(a) (b)

Fig. 4. (a) The real, $\mathbb{R}e[\Lambda_2(r, I)]$ and, (b) imaginary, $\mathbb{I}m[\Lambda_2(r, I)]$, parts of the second root of $\Lambda^3 + a(r, I)\Lambda^2 + b(r, I)\Lambda + c(r, I) = 0$, as functions of r and I. The color code is: orange-red for positive, green for zero, and blue-violet for negative values.

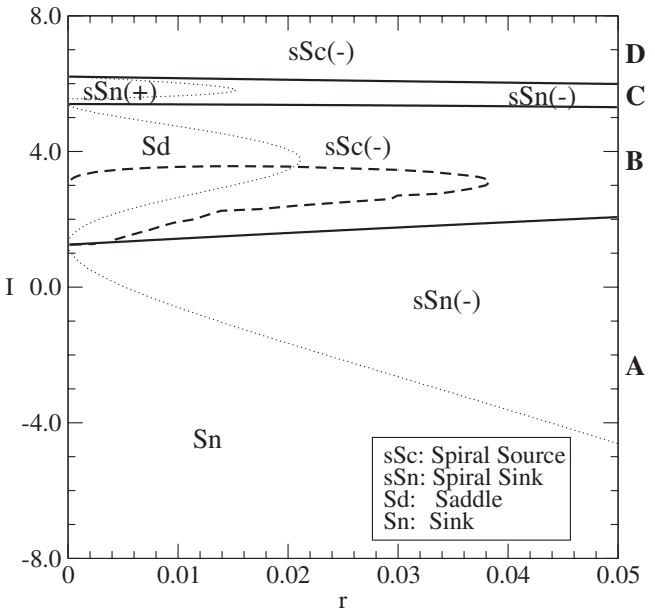

Fig. 5. Two parameter $(r - I)$ bifurcation diagram showing the different stability regimes (labeled A, B, C, D), separated by continuous lines, which represent the functions $I = \phi_i(r)$, $i = A, B, C$. The functions $\psi_A(I)$ and $\psi_B(I)$ appear as dotted lines. The dynamics observed in each region, are identified by means of abbreviations as mentioned in the figure legend, and for the case of spirals the sign of $\mathbb{I}m[\Lambda_2]$ is given in parenthesis. The dashed line is the boundary of the enclosure, $\mathcal{E}$, where complex nonlinear bifurcation structures develop (Sec. 4).

where again $\mathbb{R}e[\Lambda_{2,3}(r, I)] < 0$, is above $\phi_B(r)$ and below a third line, $I = \phi_C(r)$, that occurs around $I \approx 6.0$. Finally, for I above $\phi_C(r)$ we have region D, where $\mathbb{R}e[\Lambda_{2,3}(r, I)] > 0$. Since $\Lambda_1(r, I) < 0$ within all the rectangle $\mathcal{R}$, we have that in regions A and C the fixed point is a stable equilibrium, while in regions B and D this equilibrium is unstable.

More details on the nature of the dynamics around the fixed point are inferred from the imaginary part of the second eigenvalue, $\mathbb{I}m[\Lambda_2(r, I)] = -\mathbb{I}m[\Lambda_3(r, I)]$. This is presented in Fig. 4(b), which shows that, regarding the imaginary part of $\Lambda_2(r, I)$ and $\Lambda_3(r, I)$, the above regions, A, B and C, are separated in a left and a right zone by curves, $r = \psi_a(I)$, defined for $I \in (-4.8, 5.4)$, and $r = \psi_b(I)$, defined for $I \in (5.4, 6.1)$. The first of these curves, which has the shape of an oscillation, separates regions where $\mathbb{I}m[\Lambda_2(r, I)] = 0$ (green) from regions where $\mathbb{I}m[\Lambda_2(r, I)] < 0$ (blue); whereas, $\psi_b(I)$, which is defined for larger values of I, separates regions where $\mathbb{I}m[\Lambda_2(r, I)] > 0$ (red) from regions where $\mathbb{I}m[\Lambda_2(r, I)] < 0$ (blue). From the shape of $\psi_a(I)$ and $\psi_b(I)$ we see that in the stable region, A, it is $\mathbb{I}m[\Lambda_2(r, I)] = 0$ to the left, and $\mathbb{I}m[\Lambda_2(r, I)] < 0$ to the right; so to the left the equilibrium is a sink and to the right it is a spiral sink. For the unstable region B it is also $\mathbb{I}m[\Lambda_2(r, I)] = 0$ to the left, and $\mathbb{I}m[\Lambda_2(r, I)] < 0$ to the right; so to the left there is a saddle and to the right a spiral source. For the stable region C it is $\mathbb{I}m[\Lambda_2(r, I)] > 0$ to the left, and $\mathbb{I}m[\Lambda_2(r, I)] < 0$ to the right; so in the two cases we have spiral sinks. Finally, the whole region D is characterized by $\mathbb{I}m[\Lambda_2(r, I)] < 0$, so the dynamics there is that of a spiral source.

4. Nonlinear Analysis

More insight on the nature and stability of the dynamical behaviors available to the Hindmarsh–Rose model has been obtained, going beyond linear stability, by means of the calculation of the spectra of Lyapunov exponents, $\lambda_i(r, I)$ with $i = 1, 2, 3$. These have been obtained numerically using standard techniques for systems of differential equations [Wolf *et al.*, 1985]. The initial condition for such calculations were far from the equilibrium point, so that they describe the nonlinear dynamics of the system.

The results for the largest Lyapunov exponent presented in Fig. 6 allow us to distinguish the different dynamical attractors available: an equilibrium when $\lambda_1(r, I) < 0$, a cycle when $\lambda_1(r, I) = 0$, and chaos when $\lambda_1(r, I) > 0$. A check of the sign of the second Lyapunov exponent, $\lambda_2(r, I)$, allowed us to exclude the possibility of quasiperiodic motion for the $\lambda_1(r, I) = 0$ cases. Because the Lyapunov exponents are computed numerically, we never obtain an exponent that is zero with infinite precision; therefore an exponent, λ, is considered to be zero when $0_- < \lambda < 0_+$, with 0_- and 0_+ constant numbers with small absolute values given by the statistical errors involved in the calculation which are of the order of 10^{-3}. As shown in Fig. 6(a), for I below the critical line $I = \phi_A(r)$ the dynamics falls to an stable fixed point, in agreement with the results of linear stability analyses. For I above $\phi_A(r)$, we obtain cycles and chaotic dynamics interwoven in complex structures, that occur mainly for small values of r and $I > 0$, as shown in detail in Fig. 6(b). Chaotic dynamics, which occurs in region B, mainly appears in areas having the shape of vertical strips that merge on a line with small slope that goes from $(r, I) \approx (10^{-4}, 3.1)$ to $(r, I) \approx (6 \cdot 10^{-3}, 3.4)$ in the $r - I$ plane.

The long-term linear and nonlinear dynamics do not match in region C, where there is bistability

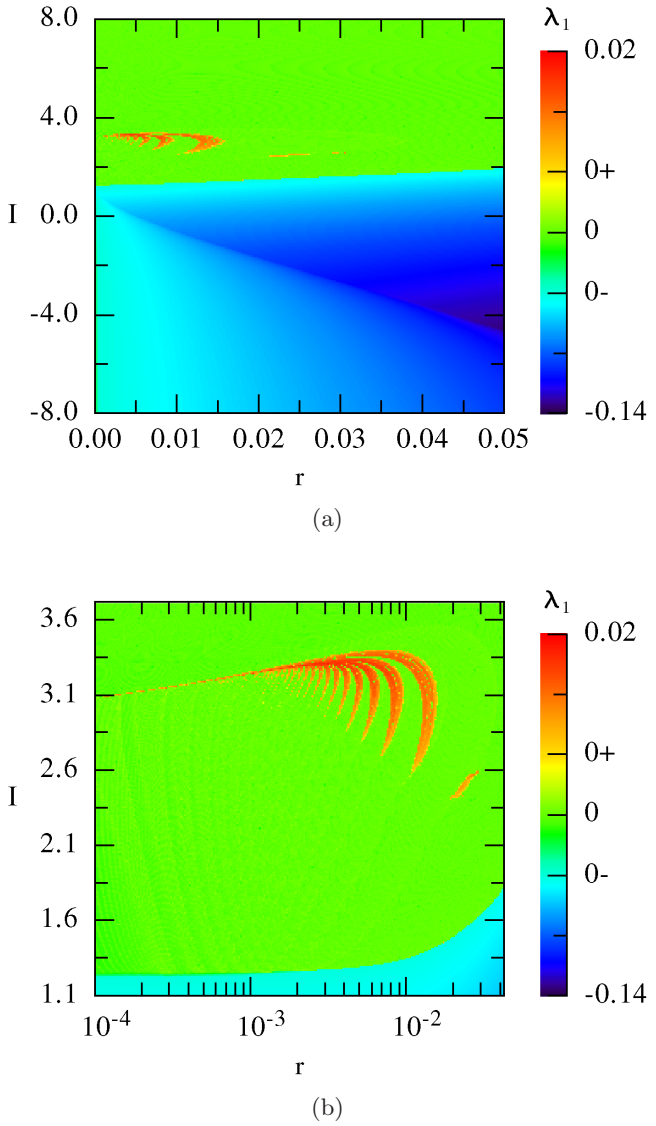

Fig. 6. The largest Lyapunov exponent, $\lambda_1(r, I)$, for Eqs. (1)–(3), as functions of r and I: (a) in the rectangle $\mathcal{R}$, and (b) in a smaller region, $\mathcal{R}_1$, where the dynamical behavior is more complex. The following color code is used: orange-red for chaotic dynamics, green-yellow for limit cycles, and violet-blue for fixed points. The interval where an exponent is considered to be zero is given by $0_- = -10^{-3}$ and $0_+ = 10^{-3}$.

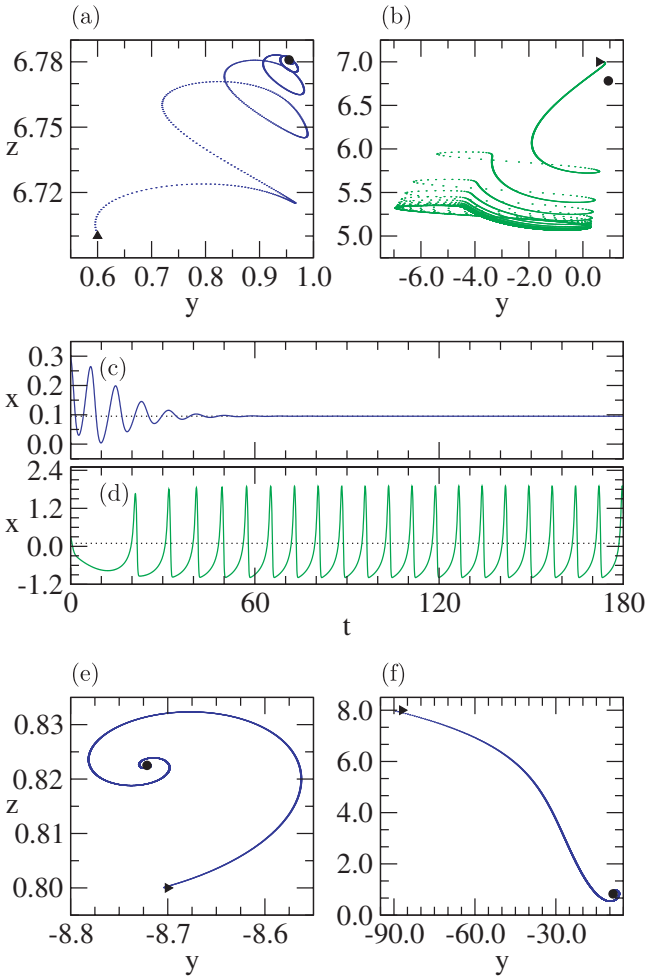

Fig. 7. (a, b) Projections of trajectories onto the $y-z$ plane of the phase space, and (c, d) time series in the bistable region C, for $r = 0.03$, $I = 5.8$ and initial conditions (a, c) $(0.3, 0.6, 6.7)$ and (b, d) $(0.3, 0.6, 7.0)$. Projections of trajectories onto the $y - z$ plane for $r = 0.03$, $I = 1.0$ and initial conditions (e) $(-1.4, -8.7, 0.8)$ and (f) $(14.0, 87.0, 8.0)$. The position of the fixed point is indicated by a filled circle in the phase space projections of trajectories, and by a dotted line in the time series plots. Filled triangles indicate the initial condition of each trajectory in phase space projections.

associated to the initial conditions that can lead the system to an equilibrium state or to periodic oscillations. This is illustrated by means of two examples in Fig. 7. The bistable behavior is shown by means of the plots of two trajectories, computed for $r = 0.03$ and $I = 5.8$, that were started at very close initial conditions, $X_0 = (x_0, y_0, z_0)$. For $X_0 = (0.3, 0.6, 6.7)$, the projection of the phase space trajectories onto the $y - z$ plane [Fig. 7(a)], and the time series for $x(t)$ [Fig. 7(c)] show an oscillatory decay towards the fixed point located at $X_F = (0.095, 0.955, 6.781)$. Whereas for $X_0 = (0.3, 0.6, 7.0)$, the system is attracted to a limit cycle in phase space [Fig. 7(b)], regarding the action potential this means a time series made from a periodic firing of a pulse [Fig. 7(d)].

This is contrary to what happens in the other linearly stable region (region A), where no matter if the initial conditions are close or far from the fixed point the dynamics tends asymptotically to the equilibria. This is illustrated in Figs. 7(e) and 7(f) by means of projections of phase space trajectories computed for $r = 0.03$ and $I = 1.0$ and initiated at $X_0 = (-1.4, -8.7, 0.8)$ and at

$X_0 = (-14.0, -87.0, 8.0)$, respectively. Since the fixed point at $X_F = (-1.394, -8.721, 0.822)$ the two trajectories share the same fate.

The dynamics in region D is quite simple: we have a stable limit cycle and an unstable equilibrium point; trajectories escaping from this drop into the cycle.

From these results, we see that it is region B, in the parameter plane, where the dynamical behavior of the Hindmarsh–Rose model is more complex, and then more interesting. More precisely, the rectangle

$$\mathcal{R}_1 = \{(r, I) | r \in [10^{-4}, 0.04] \text{ and } I \in [1.1, 3.7]\}, \tag{12}$$

contains the values of the parameters that lead to complex periodic oscillations (i.e. bursts and spikes) and chaos. Then, we will concentrate now on this rectangle. The main feature of this complexity is block structured dynamics [González-Miranda, 2005], which can be characterized by the periodicity of the oscillations of $x(t)$, and is suggested by the strip-like appearance of the areas of chaotic motion. To explore this behavior, we have computed a large number of one-dimensional bifurcation diagrams like those in Fig. 2. To have a global view of all of them we define the width of the bifurcation diagram at point (r, I) as

$$W(r, I) = T_M(r, I) - T_m(r, I), \tag{13}$$

with $T_M(r, I)$ and $T_m(r, I)$ the maximum and minimum inter-spike interval observed for (r, I), respectively. This is a measure of the dispersion of the inter-spike intervals for each point of the parameter space.

We display the results obtained in Fig. 8(a) by means of a 3D-color plot of a grid of 240×240 points in $\mathcal{R}_1$. For both, period-1 orbits and fixed points, the width of the bifurcation diagram is constant and equal to zero. This appears in Fig. 8(a) as an outer region, displayed as a flat violet color, which surrounds an enclosure, we will call it $\mathcal{E}$, where colors range from blue to red. The area $\mathcal{E}$ is the region of parameter space (Fig. 5) where the dynamics is more complex because the periodicity of the orbits is 2 or greater, or there is chaos. The limit of this area is made by a line that is composed by a segment of $\phi_A(r)$, in its lower part, and the curve where period-1 cycles bifurcate to period-2 cycles. This line is clearly seen as the set of points where the violet color of the outer region abruptly becomes blue or green for the period doubling bifurcation curve, or yellow-red for the curve $\phi_A(r)$.

Inside $\mathcal{E}$, the width of the bifurcation diagrams increases, steadily between three and four orders of magnitude when r decreases. When I is increased, it suffers comparatively smaller variations, except in the lower and upper limits of $\mathcal{E}$. In the lower limit, we have an abrupt change along $\phi_A(r)$ which corresponds to a Hopf bifurcation where an equilibrium point exchanges stability with a limit cycle. In the upper limit we have the continuous interior crises previously described [González-Miranda, 2003]. These are seen as a well-defined line inside $\mathcal{R}$, where a blue region suddenly

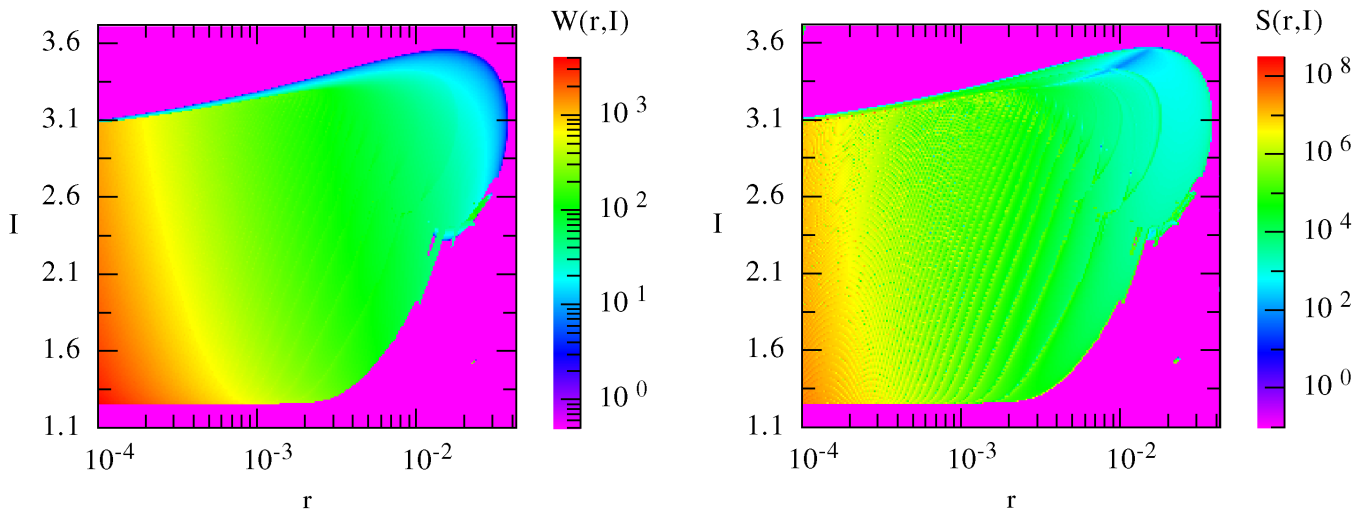

Fig. 8. (a) The width, $W(r, I)$, of the bifurcation diagram and (b) the modulus of its gradient $S(r, I)$ in the rectangle $\mathcal{R}_1$. The intensity of the color scales provides us with measures of the corresponding magnitudes.

becomes orange or light green. All this is in accordance with the particular one-dimensional bifurcation diagrams shown in Fig. 2.

More insight on the system dynamics within $\mathcal{E}$ can be obtained from the modulus of the gradient of $W(r, I)$,

$$S(r, I) = \sqrt{\left(\frac{\partial W}{\partial r}\right)_I^2 + \left(\frac{\partial W}{\partial I}\right)_r^2}. \tag{14}$$

This is suggested by one-dimensional bifurcation diagrams, like those in Fig. 2, which show what has been called block-structured dynamics. The main feature of these structures is that within a block the dynamics has a well-defined periodicity. The limits between blocks are characterized by what we might call a fine structure in $W(r, I)$: there are some abrupt tiny changes in the width of the bifurcation diagram around each period-adding bifurcation. This is a feature, only suggested in the plot of $W(r, I)$, that can be better seen from a glance at $S(r, I)$, which is displayed in Fig. 8(b). $W(r, I)$ being constant outside $\mathcal{E}$, the limits of the enclosure are also clearly seen in this plot; but, what is more important, is that we can appreciate the presence and extent of block structured dynamics. The limits of the blocks are seen as yellow lines, with slopes around 65°. Therefore, the interior of $\mathcal{E}$ can be divided in regions characterized by a given periodicity, $p \geq 2$, of the dynamics. These regions have the shape of narrow strips inclined at about 65°, where the periodicity increases, from right to left, by means of period-adding bifurcations which change p in a unit when the line is crossed. The width of the strip decreases as the periodicity increases, and they accumulate to the left of the figure. For intensities above $I = 3.1$ the cascade of period-adding bifurcations ends abruptly in an interior crises. Below this intensity our study, which was done for $r \geq 10^{-4}$, shows no end to this cascade.

This is further illustrated in Fig. 9 by means of additional plots devised to enhance the visualization of these issues. In Fig. 9(a) it appears the derivative $(\partial W/\partial I)_r$, as a function of $(r, I) \in \mathcal{R}_1$. This quantity has been chosen because plots of one-dimensional bifurcation diagrams, such as those in Fig. 2(a), where I is chosen as bifurcation parameter suggest that the maxima that separate blocks are sharper. This is presented as a 3D-color plot in Fig. 9(a), where the scale of the z-axis has been adjusted to better tune this fine structure by giving a black color to points where $(\partial W/\partial I)_r < 1$. This results in a series of blue-violet colored lines within $\mathcal{E}$ that signal the limits between blocks. These are clearly seen up to $p = 16$. Because the width of the block decreases with p, the blocks start to be indistinguishable for $p > 16$ when its width becomes commensurable with the resolution of the picture. This picture has been modified so

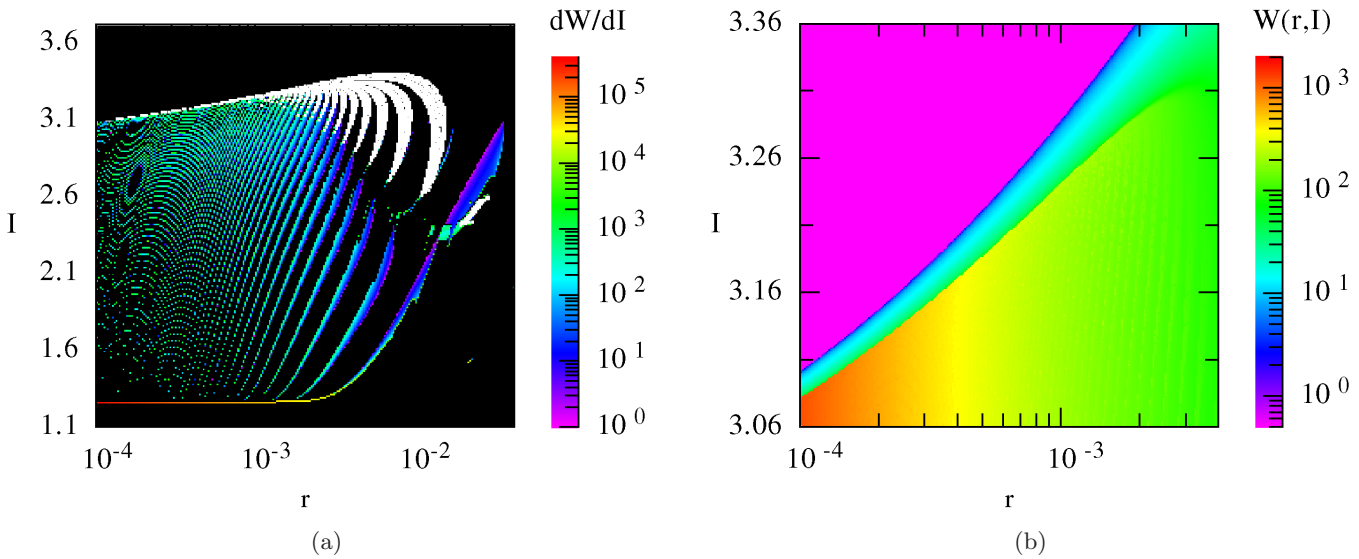

Fig. 9. (a) Derivative of the width of the bifurcation diagram with respect to I and r fixed (colored points) with the color adjusted to better display block structured dynamics. On top of this plot, as white dots, we have signaled the points where the first Lyapunov exponent is greater than zero. (b) The width, $W(r, I)$, of the bifurcation diagram around the continuous interior crisis.

that the points, (r, I), where the neuron dynamics is chaotic have been painted white to show that the strip-shaped chaotic regions match the limits between blocks. Moreover, Fig. 9(a) also shows very clearly, as a red-orange line near the bottom of the graph where Hopf bifurcations turn the equilibria to cycles.

The line where the crisis occurs, near the top of $\mathcal{E}$, is better seen in Fig. 9(b), which shows a detail of Fig. 8(a) around the crisis region. The abrupt change in the size of the attractor (between one to four orders of magnitude) is seen as a sharp line, with a slope of around 40°, that separates blue-green from red-yellow regions. The upper blue-green region corresponds to the inverted period doubling cascade that leads to period-1 cycles that lie in the violet region. The lower orange-yellow-green regions is where block structured dynamics occurs. The crises are the transition points between these two qualitatively different nonlinear dynamics. The abruptness of the crises decreases steadily as r increases, and for $r \approx 3 \cdot 10^{-3}$ we can hardly speak of such crises.

5. Structural Stability

Despite I and, sometimes, r are the control parameters that are allowed to change in most of the published research involving the Hindmarsh–Rose model; there are two other parameters that can be taken into consideration. As originally written by Hindmarsh and Rose [1984], Eq. (3) reads

$$\dot{z} = r[s(x - \delta) - z], \tag{15}$$

where s and δ are additional parameters that describe details of the ion transfer through slow channels. Usually, these are held fixed at the values $s = 4$ and $\delta = -8/5$ given by Hindmarsh and Rose [1984], just as we have done here. Some authors (e.g. [He *et al.*, 2001; Rosenblum & Pikovsky, 2004]), however, have considered $\delta = -1.56$, and Hindmarsh and Rose [1984] have also given some limited attention to $s = 1$. Therefore, to study the structural stability of the results reported in this article, we have performed some additional calculations of eigenvalues, Lyapunov exponent and bifurcation diagrams in the plane $r - I$ for several values of δ and s.

Regarding linear stability analysis, fixed points are now determined from the roots of $p(x) = x^3 + 2x + sx + \alpha$, with $\alpha = -(1 + s\delta + I)$ and being, in this case, $z_F(I) = sx_F(I) - s\delta$. The coefficients b and c of Eq. (8) are now $b(r, I) = [1 + s - 6x_F(I) + 3x_F^2(I)]r + 4x_F(I) + 3x_F^2(I)$, and $c(r, I) = [s + 4x_F(I) + 3x_F^2(I)]r$. The corresponding polynomial equations have been solved as in Sec. 3.

To test structural stability under changes of δ we have computed the eigenvalues, $\Lambda_{1,2,3}(r, I)$, for $\delta = -1.4$ and $\delta = -1.8$. In Fig. 10(a) we summarize in a single plot the results for $\Lambda_2(r, I)$ when

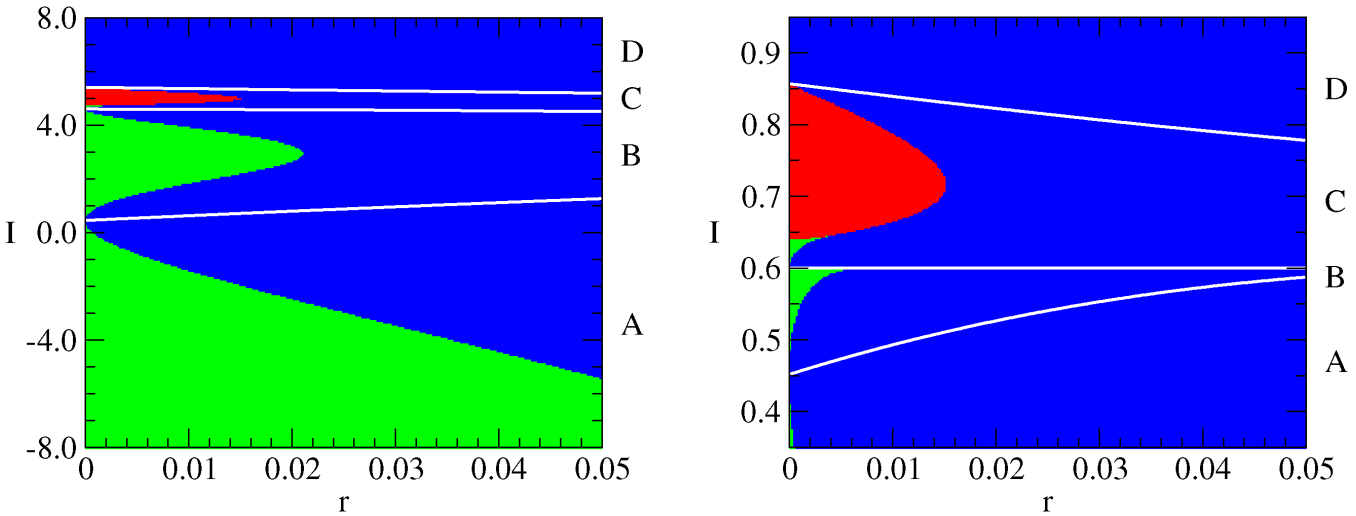

(a) (b)

Fig. 10. The imaginary part of the second root of $\Lambda^3 + a(r, I)\Lambda^2 + b(r, I)\Lambda + c(r, I) = 0$, $\mathbb{I}m[\Lambda_2(r, I)]$, plotted using the color code: red for $\mathbb{I}m[\Lambda] > 0$, green for $\mathbb{I}m[\Lambda] = 0$, and blue for $\mathbb{I}m[\Lambda] < 0$. The white lines are the functions $I = \phi_i(r)$, $i \in \{A, B, C\}$ from bottom to top, which separate stable (A, C) and unstable (B, D) regions. The parameter values modified are (a) $\delta = -1.4$, and (b) $s = 1.0$.

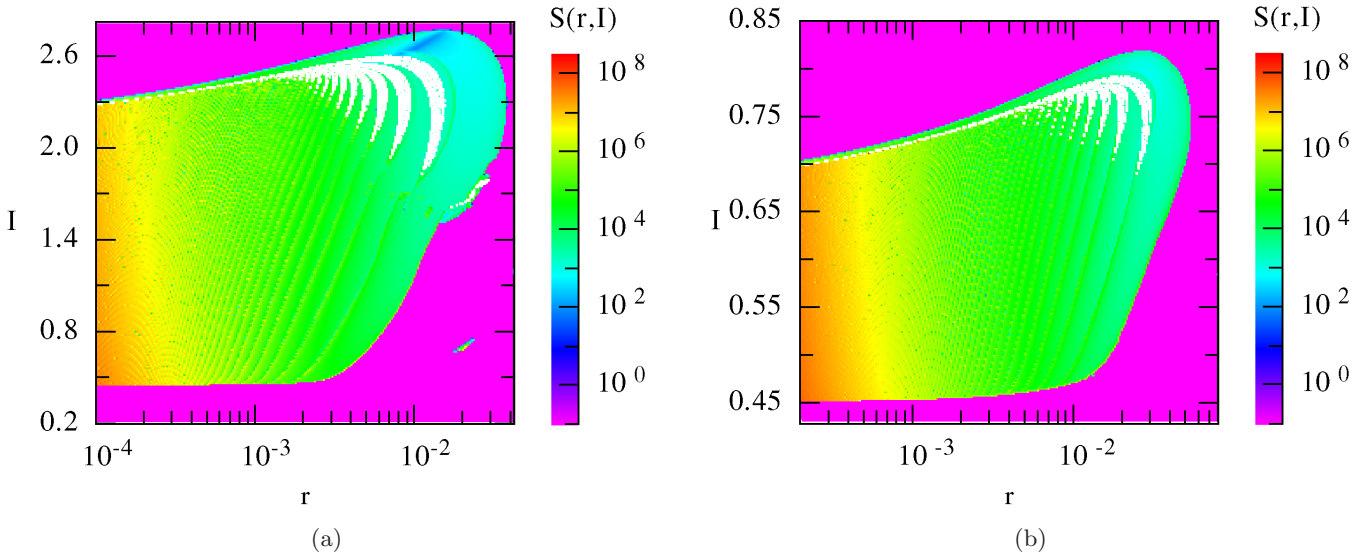

Fig. 11. Plots of $S(r, I)$, the modulus of the gradient of the width of the bifurcation diagram, for Eqs. (1)–(3), in the regions where complex bifurcation structures develop for the parameter values: (a) $\delta = -1.4$, and (b) $s = 1.0$. As done in Fig. 9(a), the points where the first Lyapunov exponent, λ_1, is greater than zero are superimposed as white dots.

$\delta = -1.4$, which are very much similar to those for $\delta = -8/5 = -1.6$, presented in Fig. 4. As in that case, $\Lambda_1(r, I)$ has been found real and negative, and $\Lambda_2(r, I)$ and $\Lambda_3(r, I)$ are complex conjugate eigenvalues, which behave in essentially the same fashion. Therefore, here we have also four alternated regions, A–D, whose stability is given by the real part of Λ_2, which have the form of horizontal strips, separated by curves $I = \phi_i(r)$, $i \in \{A, B, C\}$, with A and C as stable regions. As before, the nature of the dynamics in each region changes, depending on whether the left or right part of the strip is considered. In fact, we see nearly the same results as in Fig. 4, shifted and amount to $\Delta I \approx 0.9$ down along the I axis. The results for $\delta = -1.8$, not represented, would have looked practically the same but for a displacement of the same amount, this time up along the I axis.

The effect of s was studied by giving values to $s = 3, 2, 1$. For changes not too large, the picture given is Fig. 4, does not suffer modifications much larger than those discussed in the previous paragraph for the effect of changing δ. In particular, plots for $s = 3$ would not differ from the plots in Fig. 4 more than in Fig. 10(a). For large changes there are quantitative, but not essentially qualitative changes as illustrated by the results for $s = 1$ given in Fig. 10(b). Regarding stability we still have the two stable regions (A, C) that alternate with the unstable regions (B, D) separated by curves $I = \phi_i(r)$, $i \in \{A, B, C\}$, although the width and position of these curves have largely modified. The imaginary part of Λ_2, also presents a similar structure, except for the zone where it is zero which: (i) has been notably diminished in favor of the negative zone, to the point that it disappears in A and is much smaller in B, and (ii) has entered the lower left corner of C (we note that this last effect is also seen in Fig. 10(a), although in a much smaller scale).

The study of the Lyapunov spectrum and the two-dimensional bifurcation diagrams leads to the same kind of conclusions for the nonlinear dynamics. The results for $\delta = -1.4$, shown in Fig. 11(a) are also very much similar to those in Figs. 8 and 9. With the only exception of a small displacement of the entire figure down along the I axis, we see the same features that we founded for $\delta = -8/5$, and in particular, the complex bifurcation structures that are the signal of block structured dynamics and continuous interior crisis. For $s = 1$, Fig. 11(b) shows the same qualitative behavior seen in Figs. 8 and 9, although now they occur in a region of parameter values that is quite different.

6. Discussion and Conclusions

We have provided in this article a descriptive view of the different dynamical behaviors available to the Hindmarsh–Rose neuron model in a wide and meaningful region of its parameter space. We have determined subregions where the dynamics falls to an equilibrium point, where there are simple limit

cycles, and where there is bistability. Moreover, more importantly, we have delimited the area where the dynamics is very complex, displaying bursting periodic and chaotic firings of spikes. We have shown that there is some systematics in this region, which we describe as block structured dynamics, as well as the existence of sharp transitions from simple equilibria or periodic dynamics to this complexity. It deserves to be noted that these complex bifurcation structures most neatly develop for values of r (around 10^{-3}–10^{-2}) and I (around 1.0–4.0), which are in the vicinity of the values where the Hindmarsh–Rose model was originally fitted; thus, possibly, the most realistic.

Moreover, in our study of structural stability, we have observed that these complex bifurcation structures are also displayed by this model for other sets of parameter values. This is an indication that such structures are intrinsic fundamental properties of the Hindmarsh–Rose model. Furthermore, it has been observed [González-Miranda, 2005] that one-dimensional bifurcation diagrams like those plotted in Fig. 2, displaying block structured dynamics and continuous interior crisis, have also been observed in other models of neurons such as the Chay [1985] model and the modified Hodgkin–Huxley model of thermally sensitive neurons [Brown *et al.*, 1998]. Although, no systematic studies like the one presented here have been performed in these cases, those restricted observations suggest that complex bifurcation structures like the ones studied here might be an essential property of neuronal dynamics.

The results presented in this article provide information that is potentially useful for both improving our understanding of how neuronal systems work and to further develop the knowledge on the dynamics of nonlinear systems.

For example, abrupt changes of the dynamics such as the interior crisis and the Hopf bifurcations provide possible mechanisms to understand how a nervous system can give rapid responses to stimulus [González-Miranda, 2003] because qualitative changes of the dynamics occur in response to a small system parameter or stimulus modification. An alternative, or may be additional, mechanism for such quick responses is given by bistability, as suggested by Foss and Milton [2000], which is a phenomenon that we have also observed here. Otherwise, the neuronal coding of information needed to perform complex tasks can be performed by neurons working in the enclosure where block structured dynamics occurs as suggested by González-Miranda [2005] who proposed several coding mechanisms based on the fact that each block could be associated to a unit of meaning, and messages could be constructed by switching between these units.

Moreover, background information is provided to deal with many significant problems of nonlinear dynamics and chaos. These range from the study of the synchronization dynamics of nonlinear oscillators when the coupled oscillators are different [González-Miranda, 2004], to expand the range of applications of bifurcation theory of vector fields by using it for a deeper understanding of the variety of bifurcation scenarios described in this article [Guckenheimer and Holmes, 2002].

In conclusion, the phase diagram of the Hindmarsh–Rose model, studied in a significant and realistic domain of its space of parameters, displays a complex structure. The outer regions correspond to simple behaviors such as equilibria or limit cycles, which might be interpreted as states where the neuron is at rest or standing by. Moreover, core regions exist where different oscillatory dynamical behaviors can be classified according to their periodicity in blocks, which might be the dynamical elements implied in neuronal coding; therefore, these are the working regions of neuronal activity. The transition between core regions and outer regions can be very sharp, allowing rapid responses to stimulus. We think that these results provide useful background information to help the progress of the research on synchronization phenomena between coupled neurons as well as in the search for the neuronal coding mechanisms.

Acknowledgment

Research supported by DGI through Grant No. BFM2003-05106.

References

Abeles, M. [2004] "Time is precious," *Science* **304**, 523–524.

Birkhoff, G. & Mac Lane, S. [1996] *A Survey of Modern Algebra*, 5th edition (The Macmillan Company, NY).

Braun, H. A., Huber, M. T., Dewald, M., Schäfer, K. & Voigt, K. [1998] "Computer simulations of neuronal signal transduction: The role of nonlinear dynamics and noise," *Int. J. Bifurcation and Chaos* **8**, 881–889.

Chay, T. R. [1985] "Chaos in a three-variable model of an excitable cell," *Physica D* **16**, 233–242.

Dhamala, M., Jirsa, V. K. & Ding, M. [2004] "Enhancement of neural synchrony by time delay," *Phys. Rev. Lett* **92**, 074104.

Fitzhugh, R. [1961] "Impulses and physiological states in theoretical models of nerve membranes," *Biophys. J.* **1**, 445–466.

Foss, J. & Milton, J. [2000] "Multistability in recurrent neural loops arising from delay," *J. Neurophysiol.* **84**, 975–985.

González-Miranda, J. M. [2003] "Observation of a continuous interior crisis in the Hindmarsh–Rose neuron model," *Chaos* **13**, 845–852.

González-Miranda, J. M. [2004] *Synchronization and Control of Chaos* (Imperial College Press, London).

González-Miranda, J. M. [2005] "Block structured dynamics and neuronal coding," *Phys. Rev. E* **72**, 051922.

Guckenheimer, J. & Holmes, P. [2002] *Nonlinear Oscillations, Dynamical Systems, and Bifurcations of Vector Fields* (Springer-Verlag, NY).

He, D. H., Hu, G., Zhan, M. & Lu, H. P. [2001] "Periodic states with functional phase relation in weakly coupled chaotic Hindmarsh–Rose neurons," *Physica D* **156**, 314–324.

Hindmarsh, J. L. & Rose, R. M. [1984] "A model of neuronal bursting using three coupled first order differential equations," *Proc. R. Soc. London, Ser. B* **221**, 87–102.

Hirsch, M. W., Smale, S. & Devaney, R. L. [2004] *Differerential Equations, Dynamical Systems, and An Introduction to Chaos* (Academic Press, San Diego).

Hodgkin, A. L. & Huxley, A. F. [1952] "A quantitative description of membrane current and its application to conduction and excitation in nerve," *J. Physiol. London* **117**, 500–544.

Holmes, P. [2005] "Ninety plus thirty years of nonlinear dynamics: Less is more and more is different," *Int. J. Bifurcation and Chaos* **15**, 2703–2716.

Huang, D. [2004] "Stabilizing near-nonhyperbolic chaotic systems with applications," *Phys. Rev. Lett.* **93**, 214101.

Ott, E. [2002] *Chaos in Dynamical Systems* (Cambridge University Press, Cambridge).

Percha, B., Dzakpasu, R., Żochowski, M. & Parent, J. [2005] "Transition from local to global phase synchrony in small world neural network and its possible implications for epilepsy," *Phys. Rev. E* **72**, 031909.

Rosenblum, M. G. & Pikovsky, A. S. [2004] "Controlling synchronization in an ensemble of globally coupled oscillators," *Phys. Rev. Lett.* **92**, 114102.

Sejnowski, T. J. [1995] "Time for a new neural code?" *Nature* **376**, 21–22.

Varela, F., Lachaux, J.-P., Rodriguez, E. & Martinerie, J. [2001] "The brainweb: Phase synchronization and large-scale integration," *Nature Rev. Neurosci.* **2**, 229–239.

Wolf, A., Swift, J. B., Swinney, H. L. & Vastano, J. A. [1985] "Determining Lyapunov exponents from a time series," *Physica D* **16**, 285–317.